An Infrared and Radio Study of the Galactic Worm GW46.4+5.5

Kee-Tae Kim and Bon-Chul Koo
Department of Astronomy, Seoul National University, Seoul 151-742, Korea

ABSTRACT

In order to study the physical properties and origin of the Galactic worm GW46.4+5.5, we have carried out high-resolution ($\sim 3'$) HI and CO (J=1−0) line observations and analyzed available infrared and radio emission survey data. GW46.4+5.5 appears as a long ($\sim 8^\circ$), filamentary structure extending vertically from the Galactic plane in both median-filtered far-infrared and radio continuum maps. The I_{60}/I_{100} ratio in GW46.4+5.5 is estimated to be 0.29±0.05, which is significantly higher than the value determined for the solar neighborhood. The high ratio is consistent with a hypothesis that the dust grains in the worms have been processed by interstellar shocks. The radio continuum emission from GW46.4+5.5 has spectral index $\alpha \simeq -0.47$ and does not correlate with I_{60} except for emission at low ($|b| \leq 0.^\circ 5$) latitudes. Thus, most of the radio continuum emission is likely to be nonthermal. Our one-dimensional HI observations show that the HI gas associated with GW46.4+5.5 is mainly at $v_{\rm LSR} \simeq 15-40$ km s^{-1}. The HI gas is clumpy and we detected two molecular clouds associated with the HI peaks. The molecular clouds have large internal velocity dispersions, 8.0 and 6.6 km s^{-1}, compared to their masses, 2.8×10^3 and 1.7×10^3 $M_\odot$, which implies that they are not gravitationally bound.

Using the Leiden-Dwingeloo HI data, we identify an expanding HI supershell associated with GW46.4+5.5, which is centered on (l, b)$\simeq$(42°, 5°) with an angular size of $14^\circ\times22^\circ$ (or 340×540 pc^2 at 1.4 kpc). The supershell appears between $v_{\rm LSR} \simeq 18$ and 40 km s^{-1}, and decreases slowly in size as the velocity increases. An averaged position-velocity diagram reveals that the supershell has a central velocity of $\sim$18 km s^{-1}, giving a kinematic distance of 1.4 kpc, and an expansion velocity of $\sim$15 km s^{-1}. Assuming that it has been created by multiple stellar winds and supernova explosions, we estimate its kinematic age and the energy required to produce it to be about 5 Myr and 1.5×10^{52} ergs, respectively. The structure is also visible in median-filtered radio continuum maps, but not in the *ROSAT* maps. The observed molecular clouds might have condensed out of shock-compressed gas in GW46.4+5.5 because they are closely associated with the HI gas in velocity as well as in position. Their altitudes are 80 and 100 pc, respectively, higher than the scale height of the thin molecular gas disk. The physical properties of the clouds are very similar to those of the high-altitude clouds observed recently in sensitive wide-latitude CO surveys. Our results suggest that at least some of the high-altitude clouds might have formed in Galactic worms (or swept-up HI shells and supershells).

Subject headings: Galaxy: structure — ISM: bubbles — ISM: individual (GW46.4+5.5) — ISM: structure — radio continuum: ISM — radio lines: ISM

1. Introduction

Galactic worms are filamentary, vertical structures which look like worms crawling away from the Galactic plane in HI maps (Heiles 1984). These structures are found in the far-infrared (far-IR) as well as in HI maps (Koo, Heiles, & Reach 1992 [KHR]). KHR identified 118 Galactic 'worm-candidates' by cross-correlating the 60, 100 μm, and HI maps, and statistically examined their physical properties. The 118 structures were called worm candidates because more than half of them are at high latitudes, i.e., they depart from the original morphological definition that worms are vertical structures crawling out of the plane regardless of their origins. Individual features are wiggly and generally appear over a large velocity interval. A noteworthy feature is that 35 among the 118 structures have corresponding structures in 408 MHz continuum emission and 70% of the 35 structures appear to be associated with HII regions. The radio continuum emission is likely to be thermal for bright worms that are associated with HII regions. Heiles (1984) first suggested that the worms might be vertical parts of supershells which are quite extended in the z-direction or which have broken through the thin ($H \sim 170$ pc) gaseous disk and are thus open at the top, i.e., "chimneys" (Norman & Ikeuchi 1989). Shells and supershells have been found not only in the Galaxy but also in other spiral and irregular galaxies in the Local Group (Brinks & Bajaja 1986; Deul & den Hartog 1990; Kamphuis, Sancisi, & van de Hulst 1991; Kim, S. et al. 1998). In some edge-on spirals, worm-like vertical structures have also been directly observed (Rand, Kulkarni, & Hester 1990, 1992; Swaters, Sancisi, & van der Hulst 1997). The most probable origin of the structures is understood to be multiple stellar winds and supernova explosions in OB associations. Such structures should be filled with tenuous, hot ionized gas. The worms therefore could be pathways through which both Lyman continuum photons and hot gas escape from the thin gaseous disk so as to maintain the diffuse warm ionized medium, which is widespread up to $\sim$1 kpc from the Galactic midplane, and the hot ionized gas in the halo (Reynolds 1991; Dove & Shull 1994; Heiles, Reach, & Koo 1996). Collisions of high-velocity clouds with the galactic plane could also produce shells and supershells in certain specific cases (Tenorio-Tagle 1981).

Notwithstanding their importance in understanding the global structure and evolution of the interstellar medium, however, there are only a few detailed studies on individual Galactic worms or chimneys (Müller, Reif, & Reich 1987; Normandeau, Taylor, & Dewdney 1996; Maciejewski et al. 1996; Dennison, Topasna, & Simonetti 1997). In this paper, we report the results of a multiwavelength study of the Galactic worm GW46.4+5.5. GW46.4+5.5 is a long, filamentary structure stretching out vertically from the Galactic plane. The morphology is similar to the North Polar Spur (NPS) in the sense that the radio continuum structure is systematically shifted by $\sim 0\overset{\circ}{.}5$ from the HI (or far-IR) structure (KHR). It is likely that the NPS is composed of an inner radio continuum shell surrounding an X-ray emitting region and an outer HI shell (Borken & Iwan 1977; Heiles et al. 1980). Borken & Iwan (1977) suggested that the NPS might be a very old ($\sim 10^6$ years), large supernova remnant (SNR), but that the X-ray emission might be due to a reheating event, such as a recent ($\sim 10^4$ years) SN explosion. KHR noted that the shift between the radio continuum and the HI emission in GW46.4+5.5 may be related to the origin of the object as for the NPS. However, owing to low ($\sim 30'$) resolution, the data were inadequate for the study of the correlation at different wavelengths.

We have carried out high-resolution ($\sim 3'$) observations of GW46.4+5.5 in the HI 21 cm and CO J=1$-$0 lines, and investigated the physical properties of HI and molecular clouds associated with GW46.4+5.5. Using available survey data in infrared and radio emission, we show that GW46.4+5.5 is the vertical wall of an expanding HI supershell. The observations are described in Section 2 and the results are presented in Sections 3, 4, and 5. In Section 6, we examine the association between GW46.4+5.5 and other large-scale structures and consider the origin of GW46.4+5.5. We also discuss the origin of the observed molecular clouds. The last section contains our conclusions.

2. Observations

HI 21 cm line observations were undertaken using the 305 m telescope at Arecibo Observatory in 1990 October. The telescope has a half-power beamwidth (HPBW) of $3.'3$ and a main beam efficiency of 0.8 at 1.4 GHz. We observed both circular polarizations simultaneously using two 1024 channel correlators with 5 MHz bandwidth each, and the velocity resolution was 2.03 km s^{-1} after Hanning smoothing. Each

spectrum was obtained by integrating for 1 minute using frequency switching. We obtained a total of 9 one-dimensional cuts through GW46.4+5.5 at a set of constant Galactic latitudes given by 1°, 2°, ···, 9°. The spectra were taken at every 3′ in Galactic longitude. The positions of our one-dimensional cuts are listed in Table 1.

CO J=1−0 line observations were made in 1994 February and 1995 March using the 4 m telescope (HPBW = 2.′5) at Nagoya University in Japan. An SIS mixer receiver and a 1664 channel Acousto-Optical Spectrometer (AOS) with 40 MHz bandwidth were used. The velocity resolution was 0.66 km s^{-1} after Gaussian smoothing. The system temperature varied in the range 480−700 K during the observing sessions depending on weather conditions and elevation of the source. We first obtained 8 one-dimensional cuts in the same way as in the HI observations. Absolute-position switching instead of frequency switching was used in order to avoid contamination of the spectra by the atmospheric CO emission. The reference positions were checked to be free of appreciable ($T_{\rm R}^{*}$ < 0.1 K) CO emission. The velocity was centered at $v_{\rm LSR}$ = 40 km s^{-1}. The on-source integration time was 2 minutes and the typical rms noise level was 0.2 K per channel after smoothing. The observed regions with the reference positions are presented in Table 1. We also mapped two regions bounded by (l, b) = (45.°85−46.°70, 2.°60−3.°55) and (44.°00−45.°50, 3.°40−4.°45), where CO line emission was detected in our previous observations. We used absolute-position switching for the former and frequency switching for the latter. We were able to use frequency switching for the latter cloud because, when we observed the cloud in 1995 March, the velocity of the atmospheric CO emission was very different from that of the cloud. The beam separation was 3′. The central velocities were 27 km s^{-1} and 22 km s^{-1}, respectively. The typical rms noise level was 0.2 K per channel after smoothing. The intensity scale was calibrated with respect to the standard source S140 which was assumed to have $T_{\rm R}^{*}$=20 K (Yang & Fukui 1992).

We also used the *IRAS* coadded images (so called "BIGMAP"), which had been smoothed to 100 μm resolution (HPBW≃4′−5′), and the Effelsberg 11 and 21 cm survey data (Reich et al. 1990; Reich, Reich, & Fürst 1990). The HPBW's of the Effelsberg 100 m telescope are 4.′3 at 11 cm and 9.′4 at 21 cm, respectively.

3. Infrared and Radio Continuum Properties

3.1. Infrared Properties

Figure 1 shows the image of GW46.4+5.5 in 100 μm (grey-scale) and in 11 cm continuum emission (contour). We removed a smooth background emission from the far-IR and radio continuum maps by applying a median filter of 6°×2°. In far-IR emission, GW46.4+5.5 appears as an ∼8° long, filamentary structure, stretching straight out from the Galactic plane. It has a very narrow neck near b≃1.°5 and broadens to a width of about 2° above $b \simeq 2°$. Particularly interesting is a shell-like feature with a diameter of ∼2°, centered on (l, b)≃(46.°7, 5.°3). This structure, known as CTB 63, has been studied in the radio continuum by Caswell, Landecker, & Roger (1989), who concluded that it was not a discrete SNR because there was no sign of limb-brightening. We can also see another hole centered near (l, b)=(45.°8, 4.°1). The kinematics of the HI gas in this region will be discussed in Section 4.

In order to study the physical properties of dust grains in GW46.4+5.5, we examined the distributions of the 60/100 μm color temperature, $T_{\rm d}$, and 100 μm optical depth, τ_{100}. Here we assume that the far-IR emission is optically thin and the dust temperature is constant along the line of sight, and use only data with I_{60}≥0.25 and I_{100}≥1.00 MJy sr^{-1} to exclude data points with peculiar values for I_{60}/I_{100}, especially on the border of GW46.4+5.5. The derived $T_{\rm d}$ is dependent on n which is the index in the emissivity law, $Q_{\rm abs}(\lambda) \sim \lambda^{-n}$. For the graphite-silicate dust grain model of Mathis, Rumpl, & Nordsieck (1977), n is known to be between 1 and 2 (Hildebrand 1983; Draine & Lee 1984). We adopt n=1.5 throughout the present paper. In most regions of GW46.4+5.5, $T_{\rm d}$ ranges from 26.1 to 28.7 K, namely I_{60}/I_{100}=0.25−0.35. The average value of I_{60}/I_{100} for GW46.4+5.5 is 0.29±0.05, which is significantly higher than 0.21±0.02 for the solar neighborhood (Boulanger & Pérault 1988) but is comparable to the average value (0.28±0.03) of the Galactic worms (KHR). For comparison, the NPS has infrared colors, including I_{60}/I_{100} and I_{240}/I_{100}, indistinguishable from those of the average interstellar medium (Reach & Boulanger 1997). Since about half the emission at 60 μm is known to be attributed to small, transiently heated grains (Draine & Anderson 1985; Désert, Boulanger, & Puget 1990), the high value for I_{60}/I_{100} might suggest that GW46.4+5.5 contains a

larger fraction of small grains. The enhanced abundance of small grains appears to be consistent with a hypothesis that the dust grains in the worms have been significantly processed by interstellar shocks.

We derive the 100 μm optical depth using τ_{100}= $I_{100}/B_\nu(T_{\rm d})$, where B_ν(T) is the Planck function. The 100 μm optical depth is still proportional to the amount of dust along the line of sight (e.g., Kim, Lee, & Koo 1999), although it does not represent the usual optical depth of dust grains due to the contribution of small particles at 60 μm. In most regions of GW46.4+5.5, the range of τ_{100} is $(1-10)\times10^{-5}$, which is an order of magnitude lower than that in dark clouds (Wood, Myers, & Daugherty 1994). There are two regions where the dust temperature is considerably lower (<23 K) than the surrounding regions and where the 100 μm optical depth is very large ($\sim4\times10^{-4}$). They are respectively located at (l, b)$\simeq$(46.°3, 3.°0) and (45.°1, 4.°0). These two regions occur where molecular gas is detected, as we will show in Section 5. We derive some far-IR parameters of GW46.4+5.5 which are summarized in Table 2. It should be noted that the measurements are dependent on the size of the median filter used in the subtraction of a background emission and the boundary values.

3.2. Radio Continuum Properties

The radio continuum structure extends outward approximately vertically up to $b\sim3^\circ$ from the Galactic plane and then overlaps with the far-IR structure at higher latitudes, so that the two structures seem to be systematically shifted by 0.°5$-$1.°5 from each other. The surface brightness of the radio continuum declines dramatically near b=2° whereas it remains nearly constant at higher latitudes.

The radio continuum emission from the interstellar medium is divided into two distinct components: thermal free-free and nonthermal synchrotron emission. It is in general possible to distinguish the two components by measurement of the spectral index α ($S_\nu \sim \nu^{+\alpha}$). According to radio continuum observations of SNRs at various wavelengths, the spectral index α ranges largely between -0.8 and -0.3 except for Crab-like SNRs, which have flatter spectra (Green 1991). We estimate α for GW46.4+5.5 using the 11 and 21 cm continuum data from the formula

$$\alpha = 2 - \ln(T_{\rm b,21}/T_{\rm b,11})/\ln(\lambda_{21}/\lambda_{11}), \qquad (1)$$

where $T_{\rm b,11}$ and $T_{\rm b,21}$ are the 11 and 21 cm brightness temperatures, respectively. Since the 11 and 21 cm continuum data have different angular resolutions, we convolved the 11 cm continuum map to have the same angular resolution as the 21 cm map. We plotted $T_{\rm b,21}$ versus $T_{\rm b,11}$, and performed a least-squares fit to the data. Here the data points at $b \leq 0.°5$ are excluded because of a possible contribution from HII regions in the Galactic plane. The derived value for the spectral index is $\alpha \simeq -0.47$, which is much steeper than the value expected for thermal emission.

On the other hand, it was found that there is a strong correlation between $T_{\rm b,11}$ and I_{60} for HII regions (Broadbent, Haslam, & Osborne 1989; Moon & Koo 1994). The correlation has been used to decompose the 11 cm continuum into thermal and nonthermal components in searching for SNRs. We now examine whether or not there is a good correlation between $T_{\rm b,11}$ and I_{60} for GW46.4+5.5. Figure 2 is a plot of $T_{\rm b,11}$ against I_{60}. Open circles and crosses represent data points below and above b=0.°5, respectively. At $b \leq 0.°5$, we can see a fairly good correlation between the two quantities, especially for data points with high $T_{\rm b,11}$ and I_{60}. Additionally, the open circles lie near the solid line, which is not a fit but represents the relation obtained by Broadbent et al. (1989), $T_{\rm b,11}$=(6.4$\pm$1.7)$\times10^{-3}$ I_{60}, where $T_{\rm b,11}$ is in K and I_{60} in MJy sr^{-1}. To the contrary, at $b > 0.°5$, there is virtually no correlation between the two quantities. Almost all the data points, moreover, are located to the left of the solid line, suggesting an excess of 11 cm continuum emission. It should be noted that I_{60} is the total intensity of the 60 μm emission emanating from dust grains associated with neutral as well as ionized gas, and hence, if the continuum emission were thermal, the data points are expected to fall to the right of the solid line. Accordingly, the radio continuum emission from GW46.4+5.5 is likely to be nonthermal synchrotron emission. However, we can not exclude a possibility that it is partially thermal, because weak radio recombination line (RRL) emission was detected at several positions in GW46.4+5.5 (Heiles et al. 1996). All the detected positions but one are situated at $b \leq 1.°5$. The central velocities of the RRLs are in the range $v_{\rm LSR}$=31.7$-$43.5 km s^{-1}, which is similar to that of the HI gas.

4. HI Results

Figure 3 displays the position-velocity diagrams of the HI 21 cm line emission obtained in this work. For simplicity, we show only the data between $v_{\rm LSR}\simeq-5$ and 45 km s^{-1}. In Section 6, we compare the far-IR maps with median-filtered HI channel maps obtained from the Leiden-Dwingeloo survey data (Hartmann & Burton 1997), and find that the HI gas between $v_{\rm LSR}\simeq18$ and 40 km s^{-1} is associated with GW46.4+5.5. This velocity range is somewhat wider than that determined by KHR using the Berkeley survey data, $v_{\rm LSR}$=25−38 km s^{-1}. By comparing Figure 3 with the far-IR map in Figure 1, we see that the HI gas associated with GW46.4+5.5 is mainly at $v_{\rm LSR}\simeq20-40$ km s^{-1} for $b\leq6^\circ$ while it is mostly at $v_{\rm LSR}\simeq10-30$ km s^{-1} for $b\geq7^\circ$. As we describe in Section 6, however, the worm appears to be part of a much larger supershell with a central velocity of 18 km s^{-1}. The corresponding kinematic distances are 1.4 and 11.4 kpc. Here we use the Galactic rotation curve of Fich, Blitz, & Stark (1989), which assumes R_0=8.5 kpc and Θ_0=220 km s^{-1}. We adopt the near distance 1.4 kpc as the distance of GW46.4+5.5 because the far distance 11.4 kpc yields the unacceptably large worm-related parameters.

Figure 3 has a high (∼1.3 pc) spatial resolution and shows that the worm is clumpy. For example, at b=5°, there are two large (∼50′ or ∼20 pc) 'clumps' at (l, $v_{\rm LSR}$)=(45.°6, 32 km s^{-1}) and (47.°1, 29 km s^{-1}), while at b=6°, we see several small clumps between l=46° and 48°. An interesting feature is a ring-like structure which is centered on (l, b, $v_{\rm LSR}$)≃(45.°8, 4.°0, 25 km s^{-1}). This ring-like structure corresponds to the hole seen in the far-IR emission. Thus, its morphology and velocity structure are very similar to those of the HI shell either in expansion or contraction. If the structure were an expanding HI shell, its expansion velocity would be $v_{\rm exp}\sim5$ km s^{-1}. From the 100 μm maps, its size is estimated to be 37×24 pc^2 (1.°5×1.°0) at the adopted distance of 1.4 kpc.

The HI column density, N(HI), is proportional to the integrated HI line intensity in the optically thin case. In a separate paper (Kim et al. 1999), we have found that the 100 μm intensity is tightly correlated with the HI column density in the region of GW46.4+5.5, and that the estimated I_{100}/N(H) ratio is $I_{100}/N({\rm H})\simeq1.3$ MJy sr^{-1} $(10^{20}$ cm$^{-2})^{-1}$. From the 100 μm intensity map, we determine the total mass of GW46.4+5.5 to be 4.6×10^4 $M_\odot$. Our mass estimate includes a factor of 1.4 to account for the cosmic abundance of He.

5. Molecular Clouds Associated with GW46.4+5.5

We have detected CO emission in five regions (Table 3). They are marked by crosses in Figure 3. Each molecular cloud has an associated HI peak but its velocity is slightly different from that of the HI peak. KK99 1 and KK99 2 are unlikely to be related to GW46.4+5.5 because their velocities, 60 and −10 km s^{-1}, are significantly different from the velocity of the HI gas. KK99 3 and KK99 4 are certainly associated with GW46.4+5.5. These regions correspond to the two low-temperature regions mentioned in Section 3. Their central velocities are, respectively, 27 and 22 km s^{-1}. KK99 5 is also possibly related to the worm, although its central velocity is somewhat lower than the velocity of the worm.

We have mapped the distributions of CO line intensity in KK99 3 and KK99 4 and Figure 4 shows the results. Figures 4a and 4b have been obtained by integrating over the velocity range $v_{\rm LSR}$=18−35 km s^{-1} and 14−25 km s^{-1}, respectively. The peaks are located at (l, b)=(46.°35, 3.°05) and (45.°10, 4.°00). Peak emission spectra of the two molecular clouds are shown in Figure 5. Their line widths (FWHM) are 7.9 km s^{-1} and 5.6 km s^{-1}, which are much greater than the line width of dense cores of giant molecular clouds (GMCs), 1−3 km s^{-1} (Goldsmith 1987). The large line widths seem to be due to multiple components along the line of sight. The spectrum at (l, b)=(45.°10, 4.°00) clearly shows double-peaked structure, while the other does not show the apparent splitting of the line. The line parameters at the strong cores of the two clouds are listed in Table 4, in which Galactic coordinates, central velocity, line intensity ($T_{\rm R}^*$), and line width (FWHM) are given.

KK99 3 is elongated along the SE-NW direction and comprises two dense cores and an extended envelope. There are two local peaks in the northwestern core. The CO intensity in the dense core decreases steeply on the northern side. The far-IR surface brightness also drops there. According to the position-velocity maps, the velocity dispersion increases abruptly from the extended envelope to the cores, but the central velocity remains approximately constant.

KK99 4 consists of one dense core and an extended envelope elongated in the SE-NW direction. There is

an interesting hole, centered on (l, b)$\simeq$(44.°45, 4.°10), with a diameter of $\sim 7'$. In the channel maps, the central velocity appears to increase along the structure from the northwestern part to the eastern end of KK99 4. The core persists over a large velocity interval of $v_{\rm LSR}$=17.6$-$23.6 km s^{-1}. Figure 6 is a position-velocity diagram along the dashed line in Figure 4(b), which shows clearly the velocity gradient. However, we can also think of the possibility that there are two components with a little velocity gradient within each one, because the velocity dispersion of the western part is almost constant and the velocity dispersion of the core region is about twice that of the outer regions. In this case. the central velocities are $v_{\rm LSR}\simeq$19 and 22 km s^{-1}, respectively. Each component is spatially distinct except for the core region, i.e., one component appears above l=44.°10$-$45.°30, whereas the other is above l=44.°90$-$45.°60. One plausible explanation for this velocity structure is a cloud-cloud collision.

The integrated intensity of CO line emission, $W_{\rm CO}$, can be converted to the molecular hydrogen column density, $N({\rm H_2})$, using

$$N({\rm H_2}) \;=\; X \cdot W_{\rm CO}, \qquad (2)$$

where X is conversion factor in cm^{-2} (K km s^{-1})$^{-1}$. By comparing HI, CO, and 100 μm intensities, we have derived $X\simeq 0.70\times10^{20}$ cm^{-2} (K km s^{-1})$^{-1}$ for GW46.4+5.5 (Kim et al. 1999). This value is much smaller than the estimated value for molecular clouds in the Galactic plane, X=(1.8$-$4.8)$\times10^{20}$ cm^{-2} (K km s^{-1})$^{-1}$ (Scoville & Sanders 1987), but comparable to that for high-latitude clouds, $X\simeq 0.5\times10^{20}$ cm^{-2} (K km s^{-1})$^{-1}$ (e.g., Weiland et al. 1986; de Vries et al. 1987; Heithausen & Thaddeus 1990). If we take the derived value, the masses of KK99 3 and KK99 4 are 2.8×10^3 and 1.7×10^3 $M_\odot$, respectively. We also estimate the virial masses of the clouds using the formula

$$M_{\rm vir} \;=\; \frac{3\beta\sigma_{\rm tot}^2}{\rm G}\overline{R}, \qquad (3)$$

where $\overline{R}$ is the geometric mean radius, $\sigma_{\rm tot}=\Delta v_{\rm FWHM}/(8\ln2)^{1/2}$ is the velocity dispersion, and β is a constant which depends on the shape and density distribution of the cloud. Assuming a spherical cloud with uniform density distribution (β=5/3), the virial masses are 1.1×10^5 and 8.6×10^4 $M_\odot$, respectively. They are over an order of magnitude greater than the masses calculated from $W_{\rm CO}$, so that the molecular clouds do not appear to be gravitationally bound. Table 5 lists the physical parameters of the molecular clouds.

6. Discussion

6.1. Origin of GW46.4+5.5

Worms are thought to be the vertical walls of supershells. We have therefore attempted to find a large-scale structure associated with GW46.4+5.5 at various wavelengths, including HI 21 cm line, 408, 820, 1420 MHz radio continuum, and X-ray emission. In the Leiden-Dwingeloo HI channel maps, which are shown in Figure 7, we could identify a shell-like structure associated with GW46.4+5.5. The structure appears between $v_{\rm LSR}\simeq$18 and 40 km s^{-1}. Its diameter decreases slowly as the velocity increases. Thus the structure seems to be the receding hemisphere of an expanding HI supershell. The supershell is not distinguishable at velocities lower than $v_{\rm LSR}$=18 km s^{-1}. We can think of two explanations for these observations: either the supershell originally comprises only one hemisphere as for most other expanding supershells (Heiles 1979), or else its approaching hemisphere is hidden by local HI gas. On the other hand, most parts of the supershell lie above the Galactic plane and its center is located near (l, b)=(42°, 5°). Its lower part, which lies well below the plane at lower velocities, moves upward as the velocity increases and then overlies the plane at velocities higher than 33 km s^{-1}. Hence, this expanding HI supershell might have been produced by active events slightly above the Galactic plane and may have punched through the plane. Its top part is coherent over the entire velocity range. The supershell has an angular diameter of 14°$\times$22° at $v_{\rm LSR}\simeq$18 km s^{-1}. GW46.4+5.5 is the eastern vertical wall of the supershell, while GW39.7+5.7, another Galactic worm in the catalog of KHR, constitutes the western wall. RRLs were also detected in GW39.7+5.7 and their central velocities range from $v_{\rm LSR}$=27.2 to 43.3 km s^{-1}, which are in agreement with the velocity of GW46.4+5.5 (Heiles et al. 1996).

Figure 8 exhibits a position-velocity map averaged over the Galactic latitude range b=3°$-$7°. We can see a hollow, centered on (l, $v_{\rm LSR}$)$\sim$(42°, 18 km s^{-1}), and two protuberances near l=39° and 46°. The hole appears to be surrounded by a dense HI shell, which indicates that the HI gas in the hole might have been swept into the shell. The protuberances correspond to the two Galactic worms. Using this position-velocity

map, we estimate the central velocity of the supershell to be 18 km s^{-1}, giving a kinematic distance of 1.4 kpc. Thus its linear size would be 340×540 pc^2. The supershell seems to be situated on the near side of the Sagittarius arm. We also determine the expansion velocity to be ∼15 km s^{-1}.

The supershell is also visible in median-filtered 408, 820, and 1420 MHz continuum maps (Haslam et al. 1982; Berkhuijsen 1972; Reich & Reich 1986). The radio continuum structure forms an almost complete shell and appears to be somewhat smaller than the HI counterpart (Figure 9). We derived the spectral index α of the structure using the 408 and 1420 MHz continuum data in the same manner as in Section 3. For a region bounded by (l, b)=(38°−50°, 1°−18°), $\alpha \simeq -0.86$, implying that the radio continuum from the supershell is nonthermal. This value is comparable to those determined for large Galactic features, such as Loop I and Loop III (Reich & Reich 1988), but the index is much steeper than that obtained earlier by using the Effelsberg 11 and 21 cm continuum data. This is probably because thermal emission is present at low latitudes in GW46.4+5.5, as the detection of RRL emission suggests, and the fraction of thermal emission to nonthermal emission becomes greater at higher frequencies. On the other hand, we could not find any obvious enhancement of X-ray emission inside the supershell in the *ROSAT* $\frac{1}{4}$ keV, $\frac{3}{4}$ keV, and 1.5 keV bands (Snowden et al. 1997). Assuming that all the HI emission in the velocity range 0−18 km s^{-1} arises between us and the supershell, we estimate the foreground HI gas column density toward the center of the supershell. The derived values are (1−1.5)×10^{21} cm^{-2}, which give optical depths ∼0.5 in the $\frac{3}{4}$ keV band and ∼0.1 in the 1.5 keV band. This suggests that the absence of X-ray emission in the bands is not due to the absorption by the intervening interstellar gas. Therefore, the supershell might be too old to have X-ray emission harder than $\frac{3}{4}$ keV. The $\frac{1}{4}$ keV emission from the supershell, if any, would be absorbed completely by interstellar gas because of its high (∼10) opacity.

Figure 10 shows the distribution of molecular gas between $v_{\rm LSR}$=18 and 40 km s^{-1}, obtained from the Columbia CO survey data (Dame et al. 1987). We can see a diffuse, vertical filamentary structure extending at l∼46° and a gigantic molecular protuberance at l∼40°. The two structures are overlaid on the lower walls of the HI supershell, which are depicted by light dotted lines. There are several optical HII regions (Fich et al. 1990), radio HII regions (Downes et al. 1980; Lockman 1989), and massive star-forming regions (Churchwell et al. 1990; Plume et al. 1992; Shepherd & Churchwell 1996) inside and on the supershell. These objects reside mainly in the molecular protuberance. Figure 10 displays their positions in the (l, b) and (l, $v_{\rm LSR}$) planes. Open squares, filled triangles, and crosses represent optical, radio HII regions, and massive star-forming regions, respectively. Four SNRs, including G40.5−0.5, G42.8+0.6, G43.9+1.6, and G45.7−0.4, are situated in this area (Green 1991). They are marked by "×" symbols in Figure 10. Here we have not included HII regions and SNRs, such as W49A and W49B, that are known to be located at distances greater than 5 kpc based on HI absorption line observations. We also find four open clusters, NGC 6709, NGC 6738, Berkeley 43, and Berkeley 82 in the supershell. Open circles denote them in Figure 10. These clusters except NGC 6709 have hardly been studied. NGC 6709 is located near the center of the supershell. According to Hoag & Applequist (1965), this cluster contains no luminous star earlier than B5 and its distance is about 1 kpc, which is roughly comparable to the kinematic distance of the supershell. However, NGC 6709 is unlikely to have served to produce the supershell because its age is known to be too large, ∼10^8 yr (Loktin & Matkin 1994), in comparison with the kinematic age of the supershell derived below. Therefore, the supershell might have been created by multiple SN explosions occurring in the eastern side of the gigantic molecular protuberance or in the open clusters except NGC 6709 in its interior. It seems possible, in addition, that the active events have triggered some star-forming activity in the molecular cloud complex as in the sequential star formation model (Elmegreen & Lada 1977).

We estimate the energy required to produce the supershell and its age using theoretical models. Since the z-extent of our supershell is much greater than the scale height of the HI gas disk, we should consider the density gradient of the interstellar medium perpendicular to the galactic plane. With the use of numerical models several groups have investigated the evolution of supershells, driven by stellar winds and repeated SNe from an OB association, in various plane-stratified gas distributions (Tomisaka & Ikeuchi 1986; Mac Low et al. 1989; Igumentshchev, Shustov, & Tutukov 1990). The supershell in general grows preferentially and so becomes extended in the direction perpendicular to the galactic disk

in this case. With various energy input rates, Igumentshchev et al. (1990) have modeled the evolution of supershells in Gaussian and exponential gas disks. The disks were assumed to have a scale height of 140 pc and a midplane density of about 1 cm^{-3}. They presented an empirical expansion law for the radii of supershells in their equation (1): $R_{\rm s} = 97(t/10^6 \text{ yr})^{0.44}(\dot{E}/2\times10^{38} \text{ ergs s}^{-1})^{0.2}$ pc. The observed radius and expansion velocity of the supershell then suggest a kinematic age of $\tau_k = 0.44R_{\rm s}/v_{\rm ex} \simeq$5 Myr. By substituting this age estimate into the expansion law, we derive the energy input rate to be 1×10^{38} ergs s^{-1}, which means a total deposited energy of $\sim1.5\times10^{52}$ ergs. The dynamical parameters of the supershell are summarized in Table 6.

6.2. Origin of Molecular Clouds

We found two molecular clouds associated with GW46.4+5.5. The molecular clouds, KK99 3 and KK99 4, have similar central velocities and internal velocity dispersions (Table 5). As discussed above, they are closely associated with the HI gas in velocity as well as in position. In the large-scale CO map at 0.°5 resolution (Figure 10), the molecular clouds appear as a filamentary molecular structure extending out of the Galactic disk. The molecular filament is completely embedded in the HI filament. Hence, it is likely to be a molecular counterpart of GW46.4+5.5, i.e., a "molecular worm". This structure is similar to the one found in the prominent worm GW23.0−1.6 by Dame (1996), which extends up to a well-defined cloud at b=−1.3° from an active star-forming region in the Galactic plane. However, Dame's molecular worm is twice as large as (∼180 pc) and much more massive ($\sim6\times10^4$ $M_\odot$) than ours. Another two Galactic worms, GW30.5−2.5 and GW49.1−1.4, were found to have associated molecular clouds at high altitudes (Heiles et al. 1996), although their morphological associations were not investigated in detail.

It has been suggested that molecular clouds might form in swept-up shells and supershells (cf. Elmegreen 1987 and references therein). In this case, individual clouds might form in local HI peaks and on the whole the clouds would lie along the shell. The distribution of local high-latitude clouds provides good examples (Gir, Blitz, & Magnani 1994). McCray & Kafatos (1987) considered the formation of molecular clouds inside a supershell produced in a uniform medium by gravitational instability. According to their results, for the case of the supershell being in the snowplow phase as a result of radiative cooling or breaking through the galactic disk, the gravitational instability begins at

$$t_1 \approx 12\ E_{51}^{-1/15} n_{\rm o}^{-11/15} a_{\rm s}^{4/5} R_{100}^{-7/15} \quad \text{Myr}, \qquad (4)$$

where $E_{51} = (E_{\rm SN}/10^{51}$ ergs), $n_{\rm o}$ (cm^{-3}) is the ambient density, $a_{\rm s}$ (km s^{-1}) is the magnetosonic speed, and R_{100}=(R/100 pc) is radius at which the transition from the adiabatic phase to the snowplow phase occurs. In the velocity range $v_{\rm LSR}\geq$18 km s^{-1}, an averaged value of the N(HI) excess over the Galactic longitude range of the supershell, compared to N(HI) at other longitudes, is $\sim7\times10^{20}$ cm^{-2} (see Figure 8). Assuming that this represents all the preexisting ambient gas swept up within a line-of-sight radius of 170 pc, the original ambient gas density would be $n_{\rm o}$ ∼1.4 cm^{-3}. If magnetic pressure can be neglected $a_{\rm s}$ ∼0.5 km s^{-1} and R_{100} ∼1, t_1 ∼4.5 Myr. So, it seems that KK99 3 and KK99 4 could have condensed out of shock-compressed gas in the HI supershell.

If we take d=1.4 kpc, the altitudes of KK99 3 and KK99 4 are 80 and 100 pc, respectively. Since the scale height of thin molecular gas disk is ∼70 pc (Bronfman et al. 1988, scaled to R_0=8.5 kpc), they seem to be fairly far from the Galactic midplane. Their physical properties are intermediate between local high-latitude clouds and GMCs and so are very similar to those of the high-altitude clouds, which were identified recently by sensitive wide-latitude CO surveys in the first Galactic quadrant (Dame & Thaddeus 1994; Malhotra 1994). The origin of the high-altitude clouds is as yet poorly understood. Our results suggest the possibility that at least some of the high-altitude clouds might have formed in Galactic worms or swept-up HI shells and supershells.

7. Conclusions

It has been suggested that Galactic worms are the walls of supershells or chimneys. But their association has been rarely explored although there have been some detailed studies on a few Galactic worms. In this paper, we have shown that the well-defined Galactic worm GW46.4+5.5 is indeed the wall of a much larger ($\sim340\times540$ pc^2) supershell. There is strong evidence suggesting that the supershell is expanding at ∼15 km s^{-1}. The identification of the associated supershell led us to derive an accurate kinematic dis-

tance (1.4 kpc) to GW46.4+5.5 and its accurate physical parameters. Our results show that it is essential to identify associated supershells for the study of Galactic worms and that it is worthwhile to carry out similar analyses for other Galactic worms. Our high-resolution HI and CO observations revealed the clumpy HI structure of the worm and the associated molecular gas at HI peaks. The physical properties of the molecular clouds are very similar to those of the high-altitude clouds. The physical association of the molecular clouds with GW46.4+5.5 strongly suggests that they have formed within the supershell. A more systematic study might reveal the general association of high-altitude molecular clouds with Galactic worms (or HI supershells).

We thank Yasuo Fukui, Akira Mizuno, and the graduate students of the Department of Physics and Astrophysics, Nagoya University for their help with the CO line observations. We are very grateful to Carl Heiles and Magdalen Normandeau for several helpful comments and suggestions. This work has been supported in part by Basic Science Research Institute Program, Ministry of Education, project 1998-015-000284.

REFERENCES

Berkhuijsen, E. M. 1972, A&AS, 5, 263

Borken, R. J., & Iwan, D. C. 1977, ApJ, 218, 511

Boulanger, F., & Pérault, M. 1988, ApJ, 330, 964

Brinks, E., & Bajaja, E. 1986, A&A, 169, 14

Broadbent, A., Haslam, C. G. T., & Osborne, J. L. 1989, MNRAS, 237, 381

Bronfman, L., Cohen, R. S., Alvarez, H., May, J., & Thaddeus, P. 1988, ApJ, 324, 248

Berkhuijsen, E. M. 1972, A&AS, 5, 263

Caswell, J. L., Landecker, T. L., & Roger, R. S. 1989, AJ, 97, 1721

Churchwell, E., Walmsley, C. M., & Cesaroni, R. 1990, A&AS, 83, 119

Dame, T. M., Ungerechts, H., Cohen, R. S., de Geus, E. J., Grenier, I. A., May, J., Murphy, D. C., Nyman, L.-A., & Thaddeus, P. 1987, ApJ, 322, 706

Dame, T. M., & Thaddeus, P. 1994, ApJ, 436, L173

Dame, T. M. 1996, in Proc. IAU Symp. 170, CO: 25 Years of Millimeter-Wave Spectroscopy, ed. W. B. Latter et al. (Dordrecht: Kluwer), 19

de Vries, H. W., Heithausen, A., & Thaddeus, P. 1987, ApJ, 319, 723

Désert, F. X., Boulanger, F., & Puget, J.-L. 1990, A&A, 237, 215

Dennison, B., Topasna, G. A., & Simonetti, J. H. 1997, ApJ, 474, L31

Deul, E. R., & den Hartog, R. H. 1990, A&A, 229, 362

Dove, J. B., & Shull, J. M. 1994, ApJ, 430, 222

Downes, A. J. B., Wilson, T. L., Bieging, J. H., & Wink, J. E. 1980, A&AS, 40, 379

Draine, B. T., & Lee, H. M. 1984, ApJ, 285, 89

Draine, B. T., & Anderson, N. 1985, ApJ, 292, 494

Elmegreen, B. G., & Lada, C. J. 1977, ApJ, 214, 725

Elmegreen, B. G. 1987, in Interstellar Processes, ed. D. Hollenbach & H. Thronson (Dordrecht: D. Reidel), 259

Fich, M., Blitz, L., & Stark, A. A. 1989, ApJ, 342, 272

Fich, M., Treffers, R. R., & Dahl, G. P. 1990, AJ, 99, 622

Gir, B.-Y., Blitz, L., & Magnani, L. 1994, ApJ, 434, 162

Goldsmith, P. F. 1987, in Interstellar Processes, ed. D. Hollenbach & H. Thronson (Dordrecht: D. Reidel), 51

Green, D. A. 1991, PASP, 103, 209

Hartmann, D., & Burton, W. B. 1997, Atlas of Galactic Neutral Hydrogen (Cambridge: Cambridge Univ. Press)

Haslam, C. G. T., Salter, C. J., Stoffel, H., & Wilson, W. E. 1982, A&AS, 47, 1

Haslam, C. G. T., & Osborne, J. L. 1987, Nature, 327, 211

Heiles, C. 1979, ApJ, 229, 533

———. 1984, ApJS, 55, 585

Heiles, C., Chu, Y.-H., Renolds, K. J., & Yegingil, I. 1980, ApJ, 242, 533

Heiles, C., Reach, W. T., & Koo, B.-C. 1996, ApJ, 466, 191

Heithausen, A., & Thaddeus, P. 1990, ApJ, 353, L49

Hildebrand, R. H. 1983, QJRAS, 24, 267

Hoag, A. A., & Applequist, N. L. 1965, ApJS, 12, 215

Igumentshchev, I. V., Shustov, B. M., & Tutukov, A. V. 1990, A&A, 234, 396

Kamphuis, J., Sancisi, R., & van der Hulst, T. 1991, A&A, 244, L29

Kim, K.-T., Lee, J.-E., & Koo, B.-C., 1999, ApJ, 523, in press

Kim, S., Staveley-Smith, L., Dopita, M. A., Freeman, K. C., Sault, R. J., Kesteven, M. J., & McConnell, D. 1998, ApJ, 503, 674

Koo, B.-C., Heiles, C., & Reach, W. T. 1992, ApJ, 390, 108 (KHR)

Lockman, F. J. 1989, ApJS, 71, 469

Loktin, A. V., & Matkin, N. V. 1994, Astron. Astrophys. Trans., 4, 153

Maciejewski, W., Murphy, E. M., Lockman, F. J., & Savage, B. D. 1996, ApJ, 469, 238

Malhotra, S. 1994, ApJ, 437, 194

Mathis, J. S., Rumpl, W., & Nordsieck, K. H. 1977, ApJ, 217, 425

McCray, R., & Kafatos, M. 1987, ApJ, 317, 190

Mac Low, M.-M., McCray, R., & Norman, M. L. 1989, ApJ, 337, 141

Moon, D.-S., & Koo, B.-C. 1994, J. Korean Astron. Soc., 27, 81

Müller, P., Reif, K., & Reich, W. 1987, A&A, 183, 327

Norman, C. A., & Ikeuchi, S. 1989, ApJ, 345, 372

Normandeau, M., Taylor, A. R., & Dewdney, P. E. 1996, Nature, 380, 687

Plume, R., Jaffe, D. T., & Evans II, N. J. 1992, ApJS, 78, 505

Rand, R. J., Kulkarni, S. R., & Hester, J. J. 1990, ApJ, 352, L1

————. 1992, ApJ, 396, 97

Reach, W. T., & Boulanger, F. 1997, in The Local Bubble and Beyond, ed. D. Breitschwerdt, M. J. Freyberg, & J. Truemper, (New York: Springer-Verla), 353

Reich, P., & Reich, W. 1986, A&AS, 63, 205

Reich, P., & Reich, W. 1988, A&A, 196, 211

Reich, W., Fürst, E., Reich, P., & Reif, K. 1990, A&AS, 85, 633

Reich, W., Reich, P., & Fürst, E. 1990, A&AS, 83, 539

Reynolds, R. J. 1991, ApJ, 372, L17

Scoville, N. Z., & Sanders, D. B. 1987, in Interstellar Processes, ed. D. Hollenbach & H. Thronson (Dordrecht: D. Reidel), 21

Shepherd, D. S., & Churchwell, E. 1996, ApJ, 472, 225

Snowden, S. L., Egger, R., Freyberg, M. J., McCammon, D., Plucinsky, P. P., Sanders, W. T., Schmitt, J. H. M. M., Truemper, J., & Voges, W. 1997, ApJ, 485, 125

Swaters, R. A., Sancisi, R., & van der Hulst, J. M. 1997, ApJ, 491, 140

Tenorio-Tagle, G. 1981, A&A, 94, 338

Tomisaka, K., & Ikeuchi, S. 1986, PASJ, 38, 697

Weiland, J. L., Blitz, L., Dwek, E., Hauser, M. G., Magnani, L., & Rickard, L. J. 1986, ApJ, 306, L101

Wood, D. O. S., Myers, P. C., & Daugherty, D. A. 1994, ApJS, 95, 457

Yang, J., & Fukui, Y. 1992, ApJ, 386, 618

This 2-column preprint was prepared with the AAS LaTeX macros v4.0.

TABLE 1
POSITIONS OF ONE-DIMENSIONAL CUTS AND OFF POSITIONS

Scan Number	b (deg)	l-Range HI 21 cm line (deg)	l-Range CO J=1−0 line (deg)	OFFs[a] (l, b) (deg)
B1	1.0	42.5−48.0	43.0−45.5	(45.0, 1.5), (43.5, 2.5)
B2	2.0	43.0−45.7	43.0−46.0	(45.0, 1.5), (43.5, 2.5)
B3	3.0	42.5−48.0	44.0−47.0	(43.5, 2.5), (45.8, 4.2)
B4	4.0	43.0−47.5	44.0−46.5	(47.5, 3.5), (45.8, 4.2)
B5	5.0	42.5−50.0	45.0−48.0	(46.5, 5.3), (49.0, 5.5)
B6	6.0	42.5−51.5	46.0−48.5	(46.5, 5.3), (49.0, 5.5)
B7	7.0	42.5−51.5	46.5−47.5	(45.5, 6.5)
B8	8.0	42.5−51.0	46.5−47.5	(48.0, 8.0)
B9	9.0	42.5−51.5	···	···

[a]OFF positions for CO J=1−0 line observations

TABLE 2
FAR-IR PHYSICAL PROPERTIES OF GW46.4+5.5

Parameter	Value	Unit
Angular size in l	∼2	degree
Angular size in b	∼7	degree
Angular area	∼14	square degree
$< I_{60} >$	1.7±1.3	MJy sr^{-1}
$< I_{100} >$	6.4±4.5	MJy sr^{-1}
$< I_{60}/I_{100} >$	0.29±0.05	
$T_{\rm d}$	26−29	K
τ_{100}	(1−10)×10^{-5}	
I_{100}/N(H)	1.32±0.02	MJy sr^{-1} (10^{20} cm^{-2})$^{-1}$
τ_{100}/N(H)	1.00±0.02	10^{-5} (10^{20} cm^{-2})$^{-1}$
$M_{\rm HI}$	4.6×10^4	$M_\odot$

TABLE 3
REGIONS WITH CO J=1−0 LINE EMISSION

Cloud	b (deg)	l-range (deg)	$v_{\rm LSR}$[a] (km s^{-1})	$T_{\rm R}^{*}$[a] (K)	$\Delta v_{\rm FWHM}$[a] (km s^{-1})
KK99 1	1.0	43.50−43.70	+60	2.5	2.1
KK99 2	1.0	44.50−44.75	−10	2.1	2.9
KK99 3	3.0	45.30−46.65	+27	3.0	7.8
KK99 4	4.0	44.20−45.50	+22	3.3	5.6
KK99 5	5.0	47.65−47.95	+14	1.8	2.5

[a]Line parameters at peak position

TABLE 4
CO J=1−0 LINE PARAMETERS AT PEAK POSITIONS

	(l, b) (deg)	$v_{\rm LSR}$ (km s^{-1})	$T_{\rm R}^{*}$ (K)	$\Delta v_{\rm FWHM}$ (km s^{-1})
KK99 3				
KK99 3:P 1	(46.35, 3.05)	27.4	5.2	7.9
KK99 3:P 2	(46.20, 3.20)	27.4	4.0	8.7
KK99 3:P 3	(46.10, 3.20)	28.9	4.8	7.9
KK99 4				
KK99 4:P 1	(45.10, 4.00)	22.0	3.3	5.6
KK99 4:P 2	(44.45, 4.20)	18.5	2.8	2.5
KK99 4:P 3	(44.20, 4.20)	18.3	3.5	1.7

TABLE 5
PARAMETERS OF THE MOLECULAR CLOUDS

Cloud	$< W_{\rm CO} >$ (K km s^{-1})	$\overline{R}$ (pc)	$v_{\rm LSR}$[a] (km s^{-1})	$\Delta v_{\rm FWHM}$[a] (km s^{-1})	$M_{W_{\rm CO}}$ (10^3 $M_\odot$)	$M_{\rm vir}$ (10^4 $M_\odot$)
KK99 3	10.4	8.4	27	8.0	2.8	10.9
KK99 4	4.6	9.7	22	6.6	1.7	8.6

[a] $v_{\rm LSR}$ is the center velocity and $\Delta v_{\rm FWHM}$ is the FWHM of the composite spectral line

TABLE 6
DYNAMICAL PROPERTIES OF THE HI SUPERSHELL

Parameter	Value	Unit
Size	340×540	pc^2
Expansion velocity	$\sim$15	km s^{-1}
Kinetic age	5	Myr
Ambient density	$\sim$1.4	cm^{-3}
Total energy	1.5×10^{52}	ergs

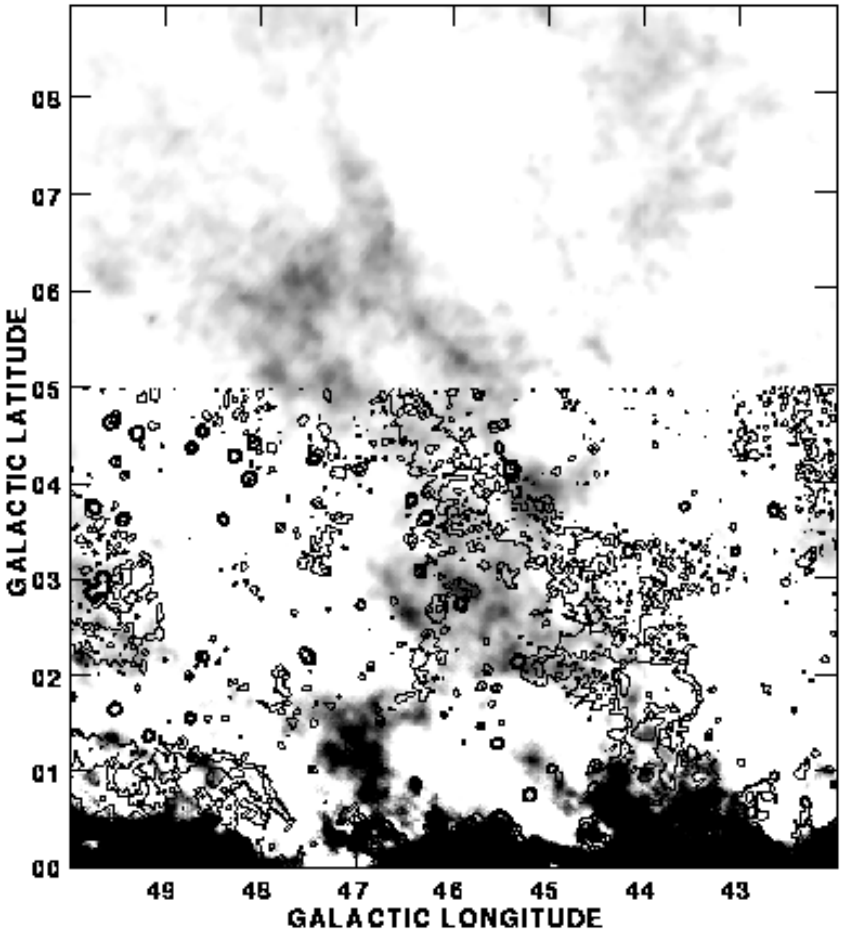

Fig. 1.— 100 μm (grey scale) and 11 cm continuum (contour) images of GW46.4+5.5. The far-IR structure extends straight up to $b = 7^\circ$ from the Galactic plane. The radio continuum structure is shifted by about 1° from the far-IR one between $b \simeq 1\overset{\circ}{.}5$ and $3\overset{\circ}{.}5$. The grey scale intensity range is 1−30 MJy sr^{-1}. Contour levels are 0.03, 0.1, 0.25, 1.0, and 3.0 K.

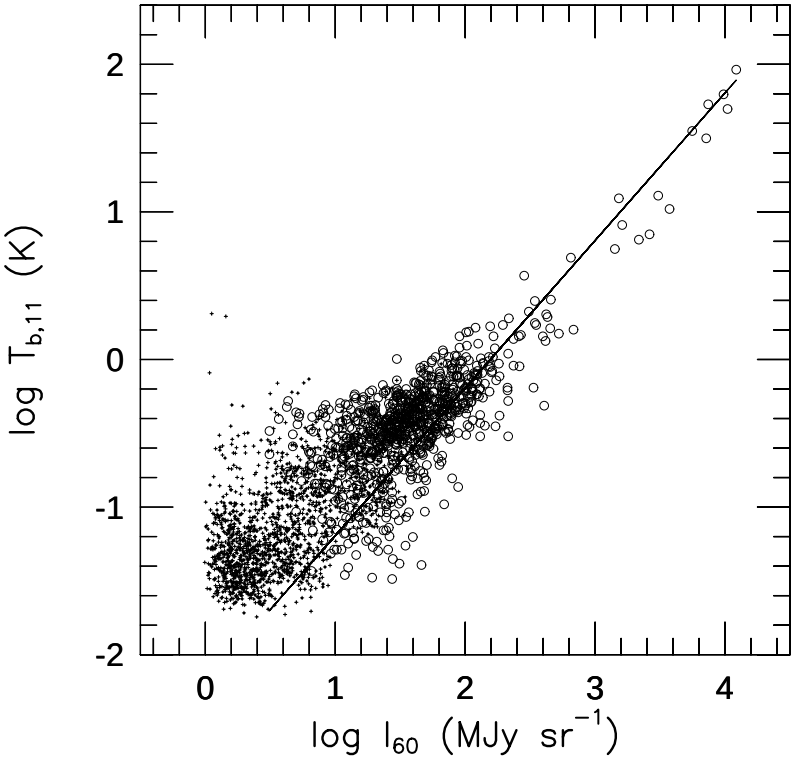

Fig. 2.— The plot of 11 cm continuum brightness temperature, $T_{\rm b,11}$, against 60 μm intensity, I_{60}. Open circles and crosses represent data points below and above b=0.°5, respectively. The solid line represents a relation between the two parameters, derived by Broadbent et al. (1989), for thermal emission.

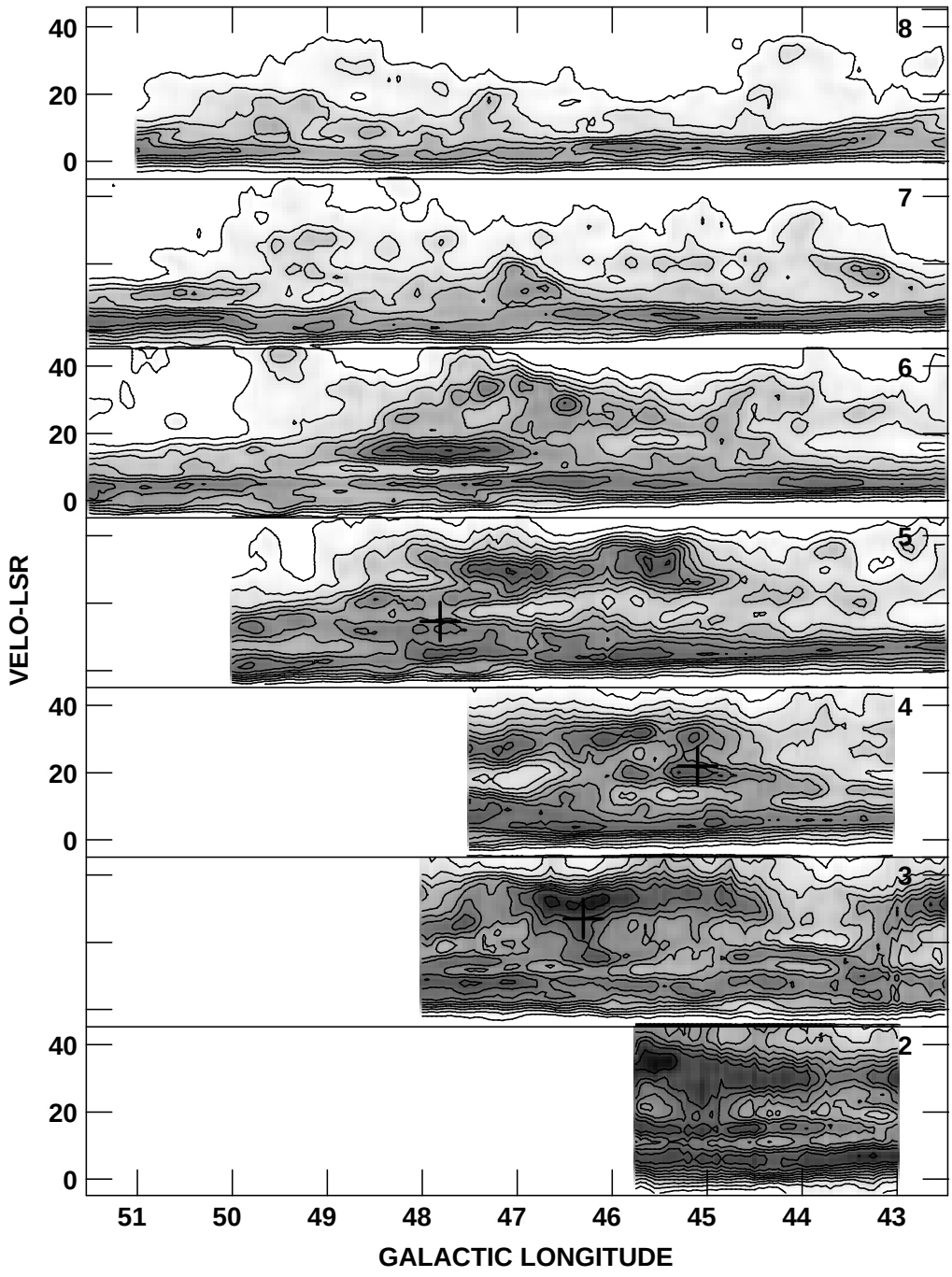

Fig. 3.— Arecibo HI position-velocity diagrams at b=2°−8°. The Galactic latitude is indicated on the top right corner of each diagram. The HI gas associated with GW46.4+5.5 is shown clearly above $v_{\rm LSR}\simeq$20 km s^{-1} at $b \leq$6°. The positions of molecular clouds detected in this work are marked by crosses. The contours correspond to 5, 10, 15, 20, 25, 30, 35, 40, 45, 50, and 60 K. The grey scale intensity range is 10−70 K.

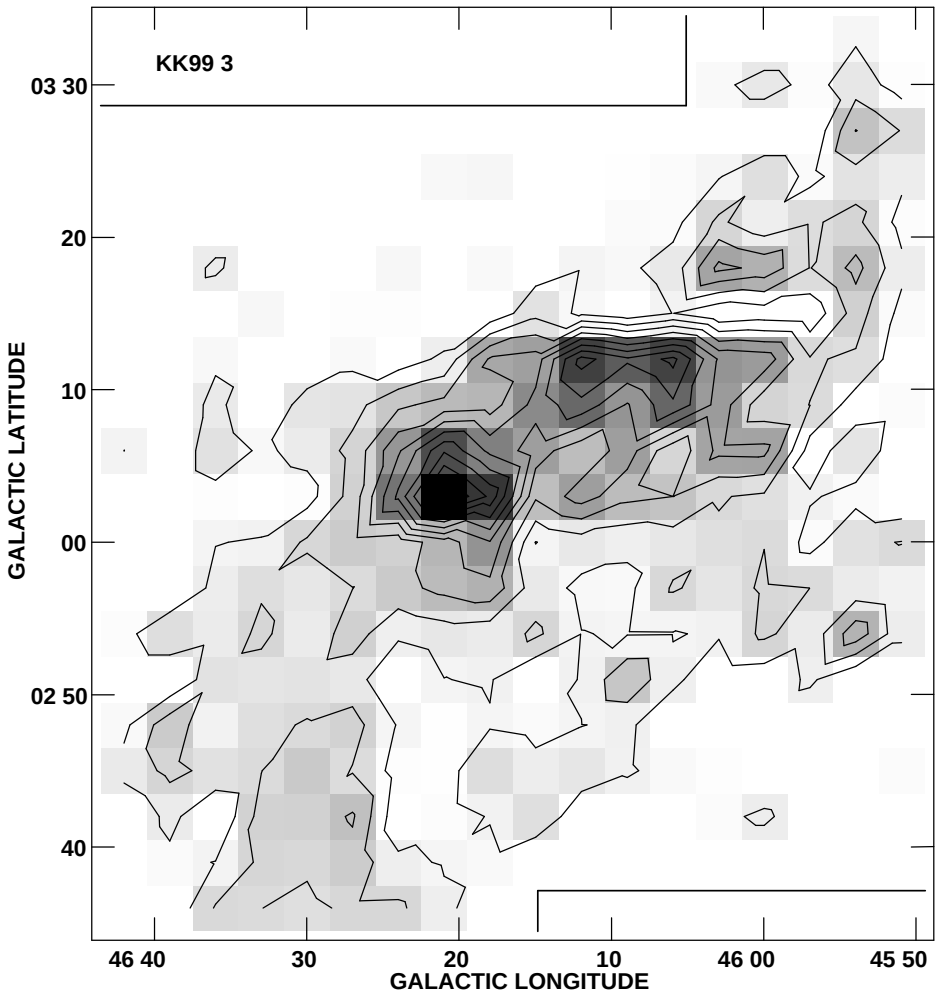

Fig. 4.— Integrated CO line intensity maps of molecular clouds 1 and 2. (a) KK99 3. The grey scale flux range is 2−44 K km s^{-1}. The distribution is obtained by integrating between $v_{\rm LSR}$ = 18 and 35 km s^{-1}. The lowest contour level and contour spacing is 4 K km s^{-1}.

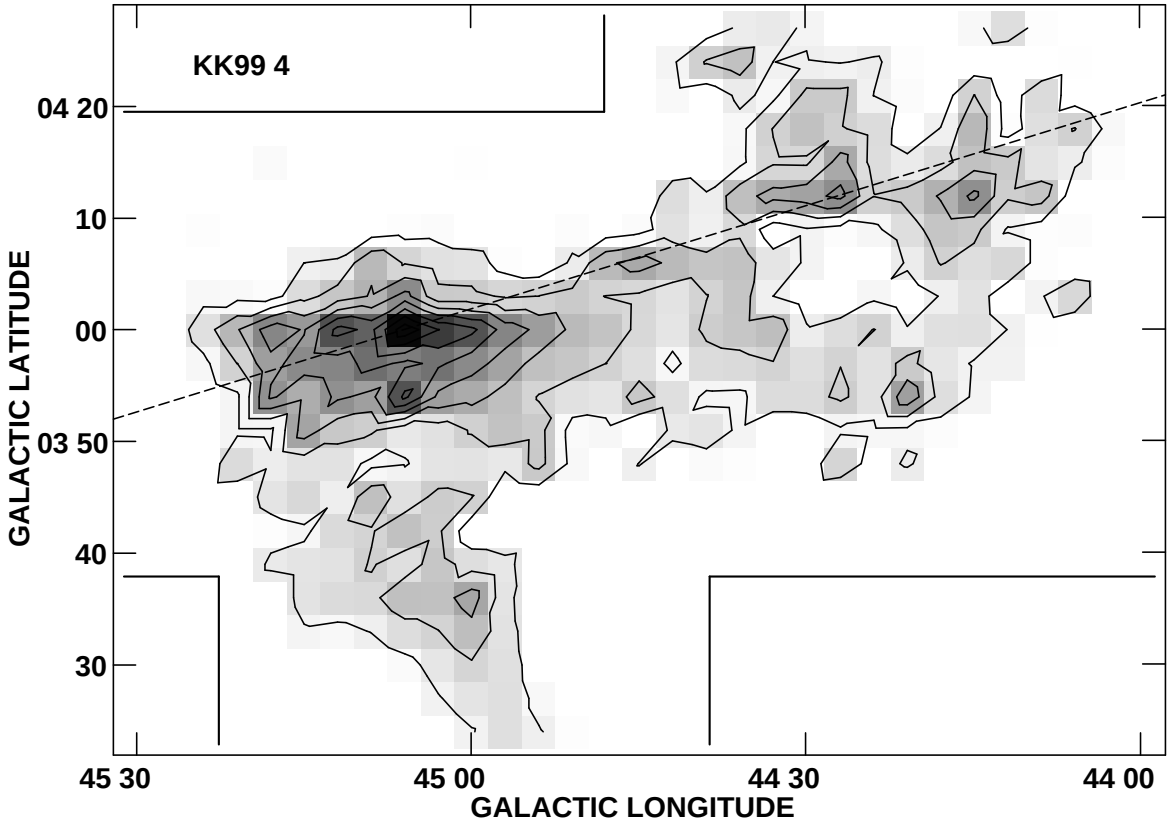

Fig. 4.— (b) KK99 4. The distribution is obtained by integrating over the velocity range $v_{\rm LSR}$=14−25 km s^{-1}. The grey scale levels range from 1 to 18 K km s^{-1}. The lowest contour level and contour spacing is 2 K km s^{-1}.

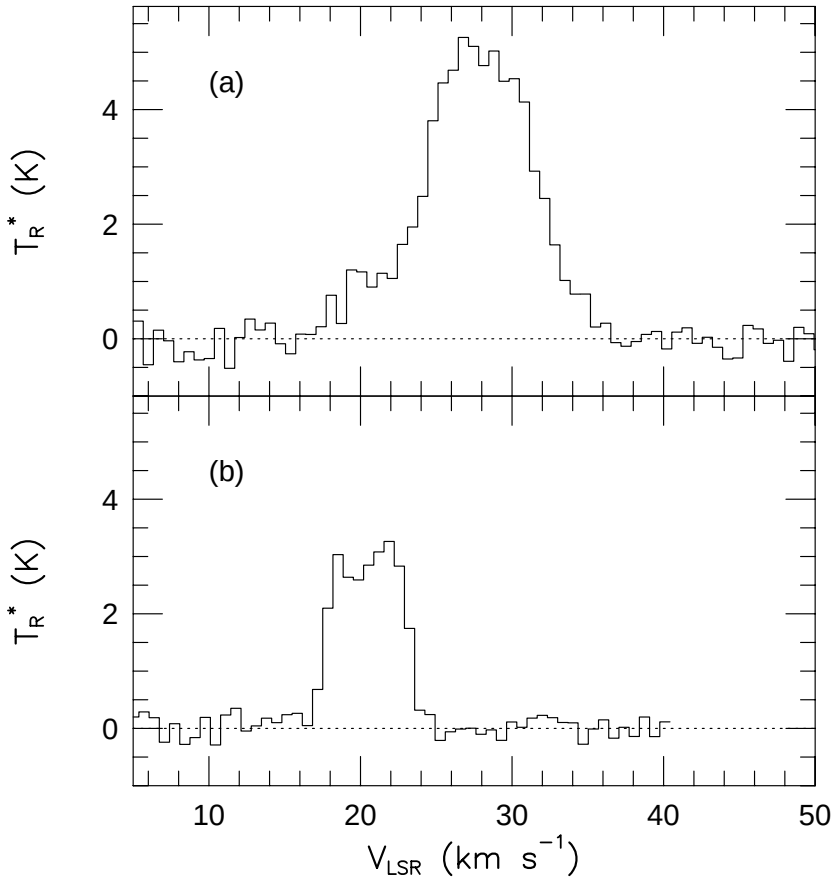

Fig. 5.— Peak emission CO line profiles (a) for KK99 3 and (b) for KK99 4. The line parameters are presented in Table 4.

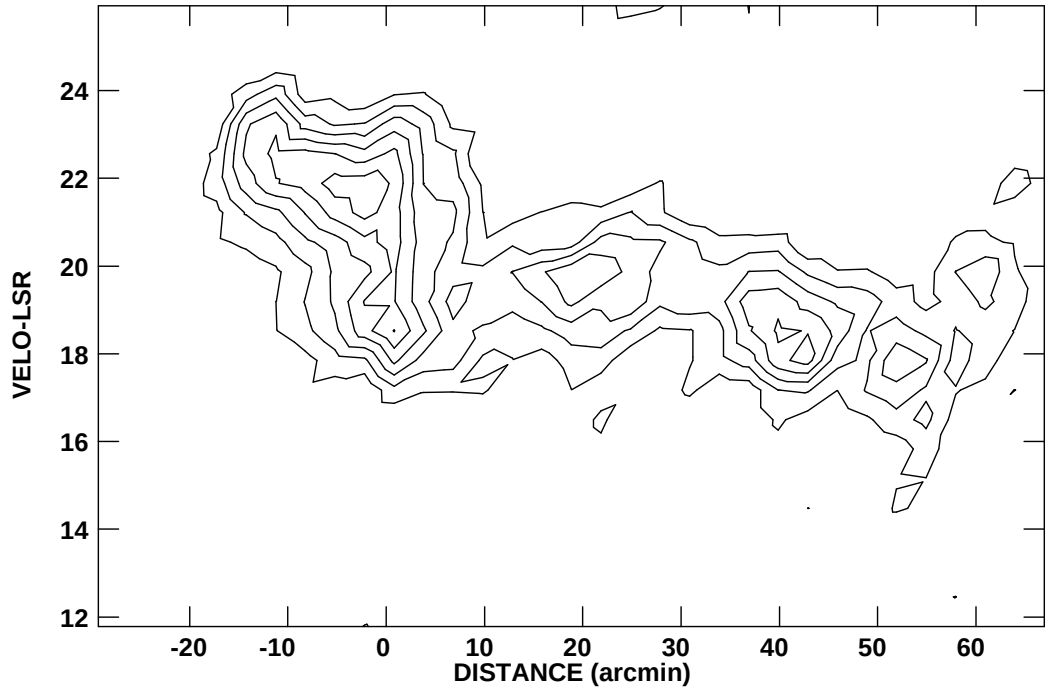

Fig. 6.— Position-velocity diagram of KK99 4 along the dashed line in Figure 4(b). The x-axis is the distance (positive toward the northwest) along the line from (l, b)=(45.°10, 4.°00). Contour levels are 0.5, 1.0, 1.5, 2.0, 2.5, and 3.0 K

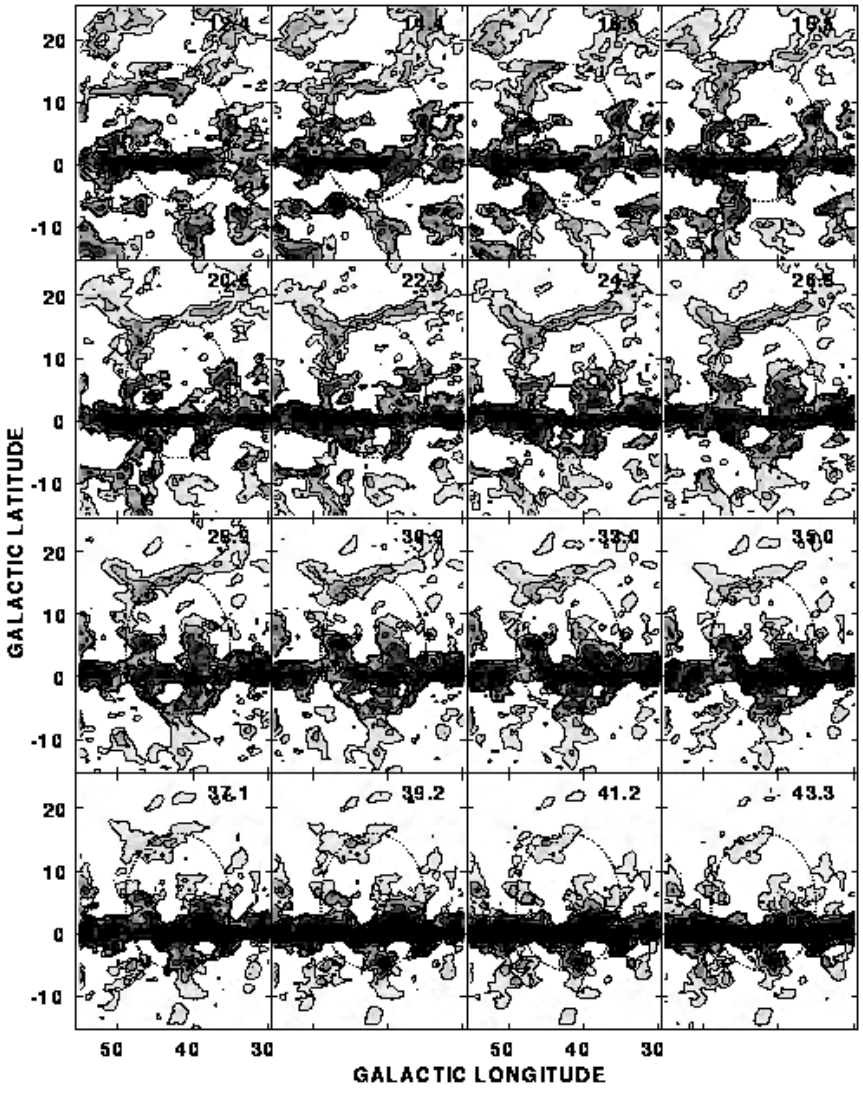

Fig. 7.— Median-filtered HI velocity channel maps, taken from the Leiden-Dwingeloo survey data. Each map exhibits the HI intensity distribution in a region of $30° \leq l \leq 55°$ and $-15° \leq b \leq 25°$. The central velocity is indicated on the top right corner in each map. The dotted ellipse centered on $(l, b)=(42°, 5°)$ represents the supershell at $v_{\rm LSR}$=18.5 km s^{-1}. The map intensity range is $T_{\rm A}^{*}$=0−25 K and contours are 1, 5, and 15 K.
(A high-quality image file lies in /pub/kimkt at the anonymous ftp site of star.snu.ac.kr.)

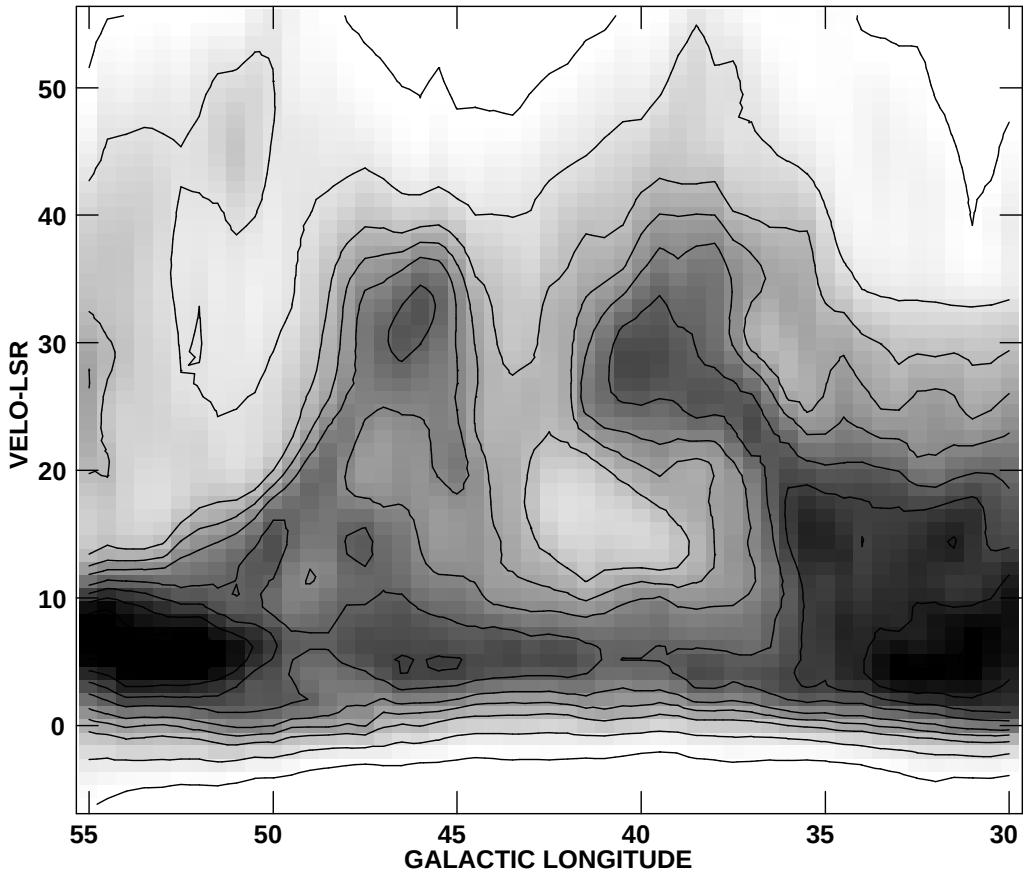

Fig. 8.— Leiden-Dwingeloo HI position-velocity diagram averaged over b=3°−7°. We can see a hole surrounded by a dense shell. The hole is centered on (l,$v_{\rm LSR}$)∼(42°, 18 km s^{-1}). Two protuberances correspond to galactic worms GW46.4+5.5 and GW 39.7+5.7, which form the vertical walls of the supershell. Contour levels are 10, 20, 32, 40, 48, 60 ,70, 80, and 90% of peak intensity, 72 K.

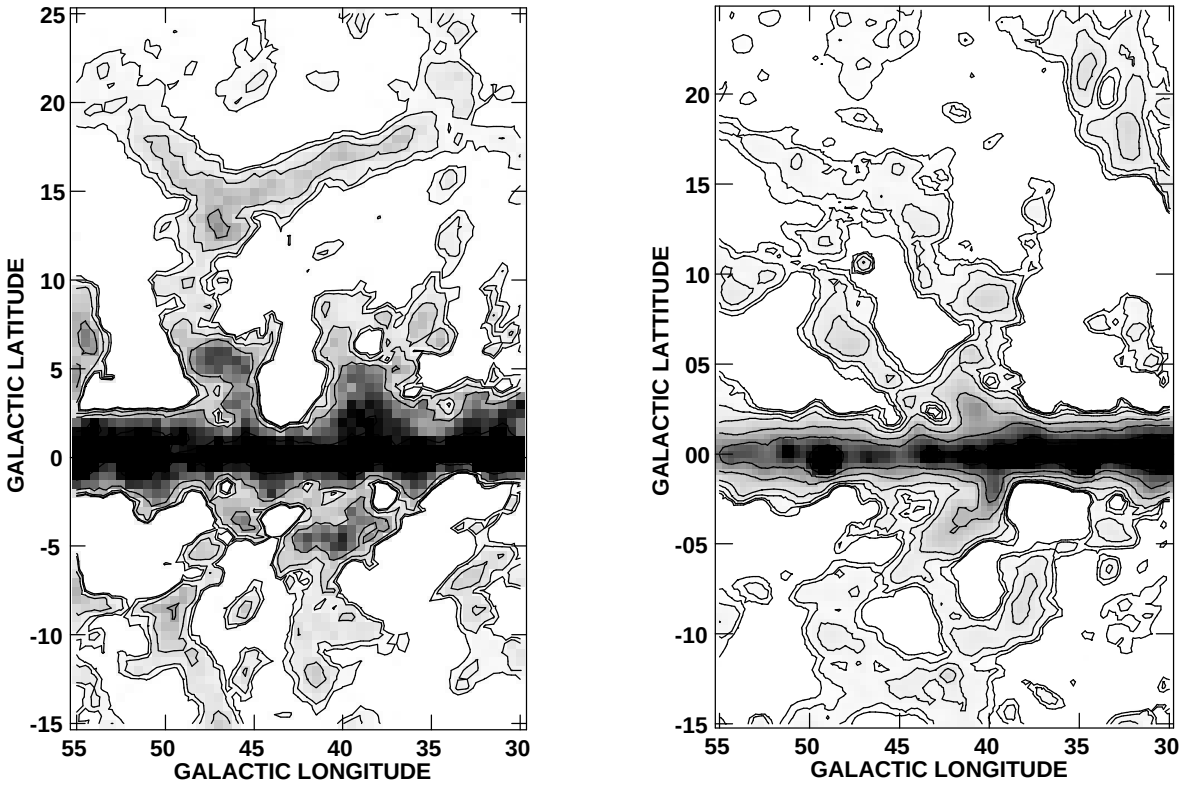

Fig. 9.— (a) Median filtered HI integrated intensity map with a resolution of 0.°5. Contour levels are 10, 30, 80, and 200 K km s^{-1} and grey scale intensity ranges from 0−600 K km s^{-1}. A shell-like structure is seen, centered on (l, b)$\simeq$(42°, 5°). (b) Median filtered 408 MHz continuum map at 0.°85 resolution. Contour levels are 0.5, 2, 5, 10, 25, 50, 100 K and grey scale intensity ranges from 0−100 K. The HI shell-like structure has a radio counterpart, which appears as an almost complete shell.

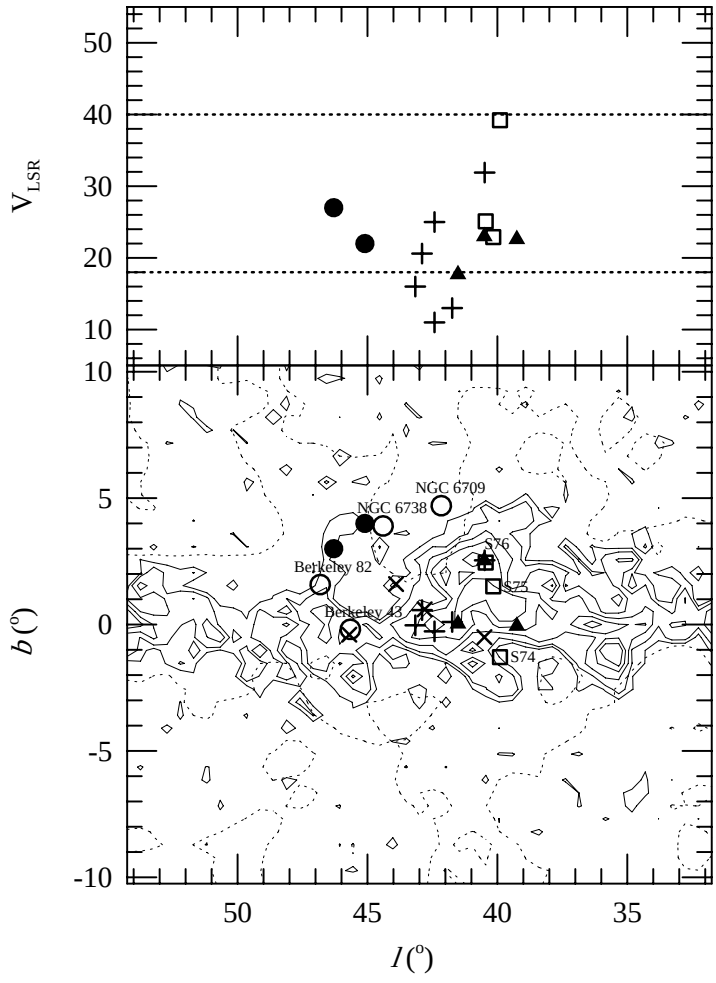

Fig. 10.— *Lower panel*: Integrated CO line intensity at 0°.5 resolution, obtained by integrating between velocities 18 and 40 km s^{-1}. Contour levels are 2.3, 5, 10, 15, and 20 K km s^{-1}. The distribution of HI column density is indicated by light dotted lines. The positions of various objects are also marked. Open circles, open squares, filled triangles, crosses, and "×" symbols represent open clusters, optical HII regions, radio HII regions, massive star-forming regions, and SNRs, respectively. Filled circles indicate KK99 3 and KK99 4, observed in this work. *Upper panel*: The distribution of various objects in the (l, $v_{\rm LSR}$) plane. Two dotted lines represent the LSR velocity range of the HI supershell.

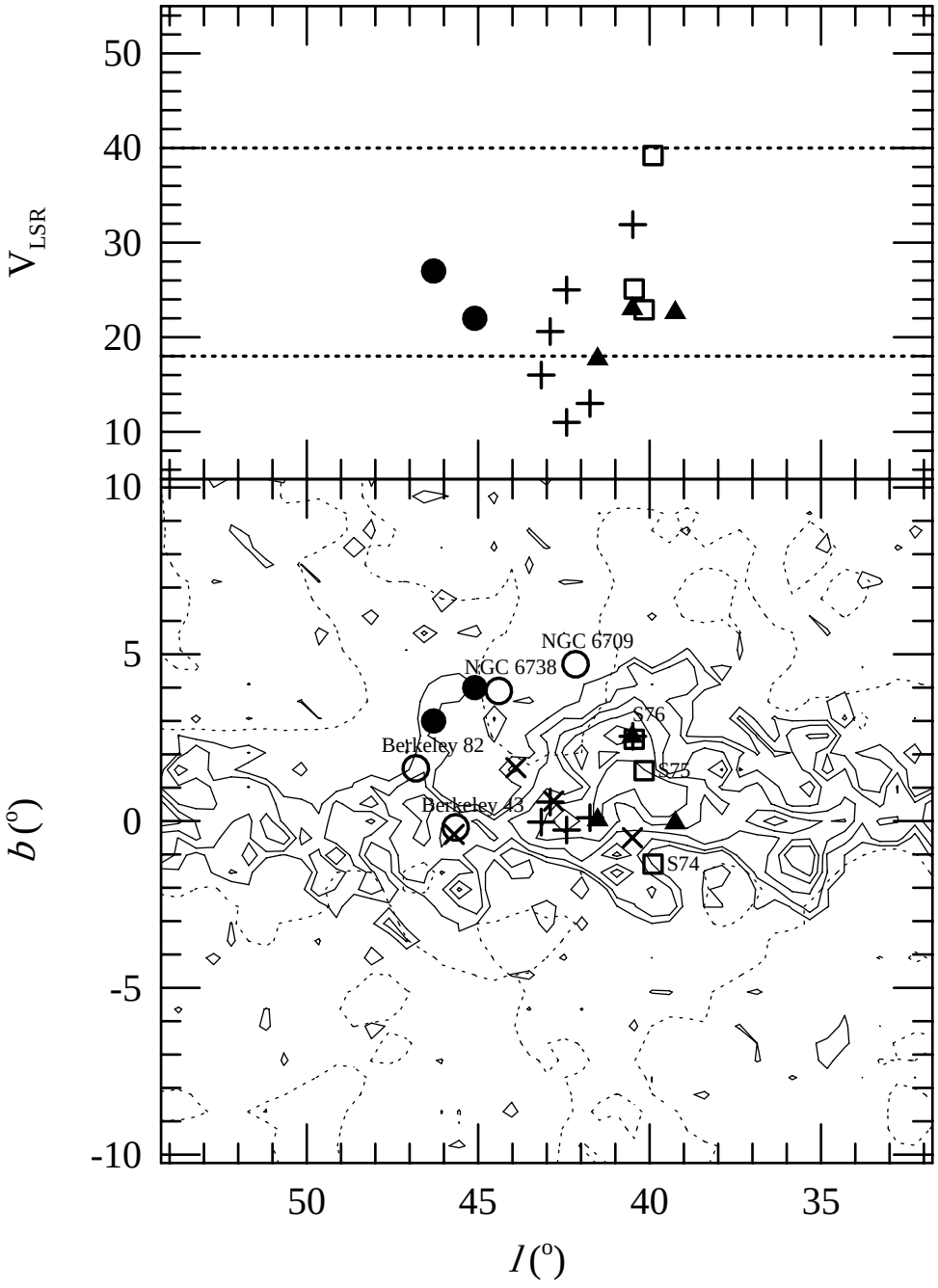
50
40
30
20
10
10
5
0
-5
-10
V_{LSR}
b (°)
l (°)
50
45
40
35
NGC 6709
NGC 6738
S76
Berkeley 82
S75
Berkeley 43
S74

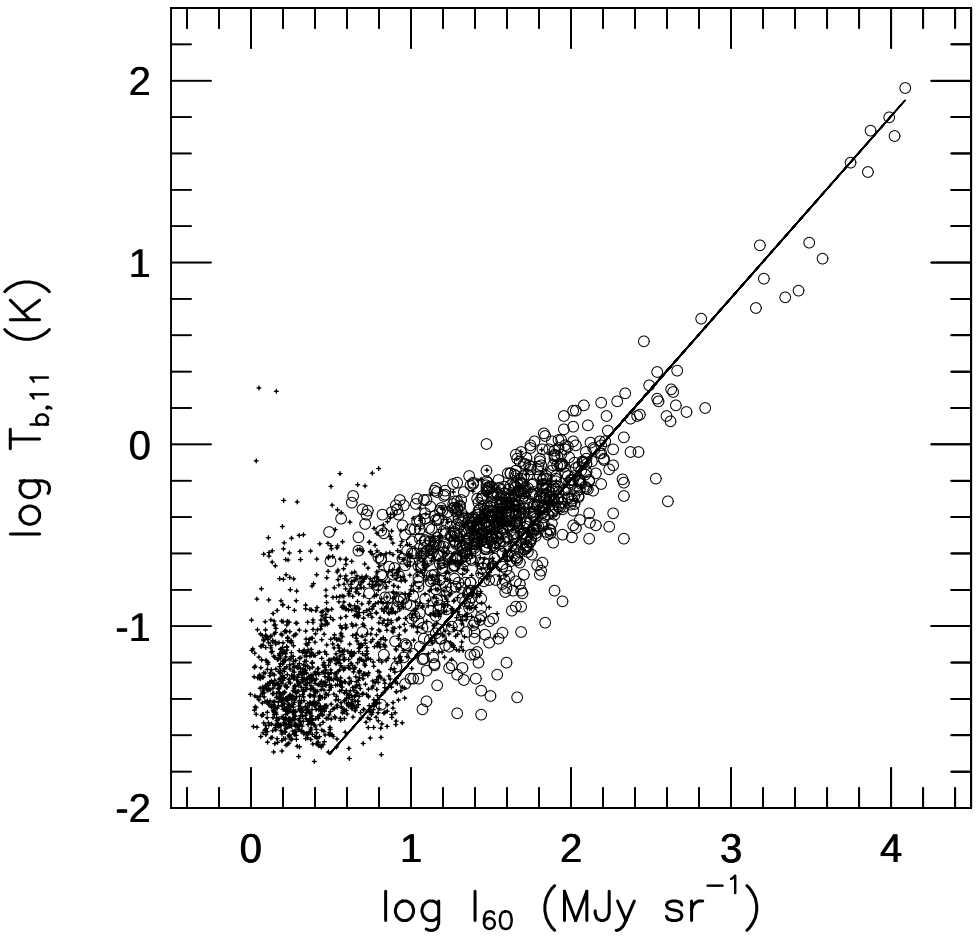
2
1
0
-1
-2
0
1
2
3
4
log $T_{b,11}$ (K)
log I_{60} (MJy sr^{-1})

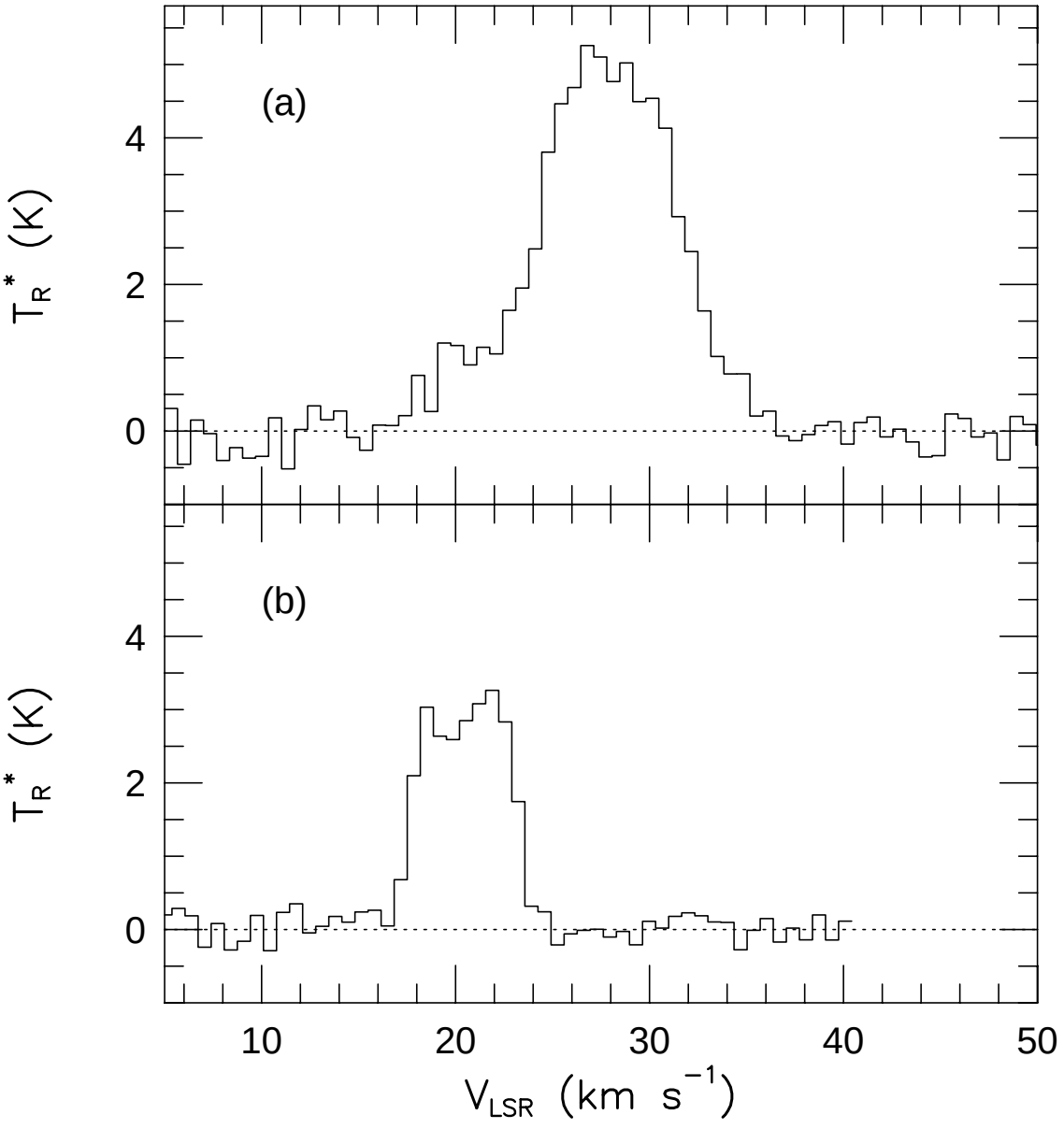
(a)
(b)
4
2
0
T_R^* (K)
10
20
30
40
50
V_{LSR} (km s^{-1})